

Accumulated Polar Feature-based Deep Learning with Channel Compensation Mechanism for Efficient Automatic Modulation Classification under Time-varying Channels

Chieh-Fang Teng, *Student Member, IEEE*, Ching-Yao Chou, *Student Member, IEEE*, Chun-Hsiang Chen, and An-Yeu (Andy) Wu, *Fellow, IEEE*

Abstract—In next-generation communications, massive machine-type communications (MTC) induce severe burden on base stations. To address such issue, automatic modulation classification (AMC) can reduce signaling overhead through blindly recognizing the modulation types without handshaking, thus playing an important role in intelligent modems. The emerging deep learning (DL) technique stores intelligence in the network, resulting in superior performance over traditional approaches. However, DL-based approaches suffer from computational complexity and offline training overhead, which severely hinder practical applications. Furthermore, the required massive resources for online retraining should be further considered under time-varying fading channel, which has not been studied in the prior arts. In this work, an accumulated polar feature-based DL with channel compensation mechanism is proposed to cope with the aforementioned issues. Firstly, the simulation results show that learning features from polar domain with historical information can approach optimal performance and reduce offline training overhead by 37.8 times. Secondly, the proposed neural network-based channel estimator (NN-CE) can learn the channel response and compensate for the distorted channel with 13% improvement. Moreover, in applying the novel NN-CE in the time-varying fading channel, two efficient mechanisms of online retraining are proposed, which reduce transmission overhead and retraining overhead by 90% and 76%, respectively. Finally, the performance of the proposed approach is evaluated and compared with prior arts on a public dataset to demonstrate its great efficiency.

Index Terms—Automatic modulation classification, polar coordinate, deep learning, convolutional neural network, fading channel, time-varying, online retraining.

I. INTRODUCTION

Fifth-generation (5G) cellular systems are expected to support over 50 billion devices by 2020, namely massive machine-type communications (MTC), which imposes a tremendous burden on base stations with the high cost of signaling overhead and energy consumption [1], [2].

To address the aforementioned challenges in enhancing the Quality of Service (QoS), software-defined radio (SDR), cognitive radio (CR), and systems with adaptive modulations have been studied extensively [3]–[8]. All of them tend to develop *intelligent modems*, having the capabilities of

spectrum sensing, self-adapting, and cooperation with neighbors, to fully utilize the available radio spectrum. To realize the intelligent transceivers, one important technology is *automatic modulation classification* (AMC), which is the intermediate step between signal detection and demodulation [9]–[12]. Based on the results of spectrum sensing, various modulation schemes are adopted to dynamically adjust transmission data rate and to meet the QoS requirement. At the receiver side, AMC is performed to blindly recognize the modulation types without prior knowledge of system parameters. Hence, with an effective AMC technology, the handshaking for exchanging *a priori* protocol information can be reduced, which results in much lower signaling overhead and better transmission efficiency [10], especially important for massive MTC.

In the past decades, various research works have been proposed in the field of AMC. They can be generally classified into two classes: likelihood-based (LB) approach [9]–[17] and feature-based (FB) approach [9]–[12], [18]–[23]. The LB approach is based on maximization of the likelihood function with the assumption of the probability density function of an incoming signal. Though LB approach can provide optimal performance in the Bayesian sense, it requires perfect knowledge of the received signals and suffers from high computational complexity. On the other hand, FB approach, the decision is based on the extracted features of the received signals, such as higher-order statistics (HOS) and power spectral density. Compared to LB approach, FB approach is simpler for implementation with near-optimal performance.

In recent years, as machine learning (ML) techniques continually demonstrate significant breakthroughs in various fields, many researchers also exploit ML techniques as classifiers with extracted features, such as support vector machine, K-nearest neighbor, and genetic programming [24]–[26]. Without extracting features in hand-engineered, deep learning (DL) can automatically learn the high-level features, and therefore has received much attention due to its superior performance in recognition tasks with complex and deep architecture [27]–[36]. For example, one-dimensional convolutional neural network is exploited in [28], [30], [32], [36] to achieve promising performance with only raw IQ samples. Furthermore, [31] maps the received symbols to scatter points on the complex plane as the input for two-dimensional CNN with better performance as shown in Fig. 1(a).

However, three critical issues of deep learning-based approaches are required to be addressed in practice:

This work is financially supported by the Ministry of Science and Technology of Taiwan under Grants MOST 105-2622-8-002-002, and sponsored by MediaTek Inc., Hsin-chu, Taiwan.

The authors are with the Graduate Institute of Electronics Engineering and Department of Electrical Engineering, National Taiwan University, Taipei, 106, Taiwan (e-mail: {jeff, endpj, johnnychen}@access.ee.ntu.edu.tw; andyw@ntu.edu.tw).

TABLE I
COMPARISON OF AUTOMATIC MODULATION CLASSIFICATION FRAMEWORKS

Frameworks	Resource Consumption			Performance	
	Online Inference	Offline Training	Online Retraining	Under Ideal Channel	Under Channel Variation
Likelihood-based (LB) [13]-[17]	×	-	-	⊙	×
Feature-based (FB) [18]-[23]	⊙	-	-	△	△
Deep Learning-based [27]-[35]	×	×	×	○	△
Proposed Accumulated Polar Feature with NN-CE	○	○	○	○	○

⊙: Optimum, ○: Good, △: Medium, ×: Bad

- 1) *Computational complexity*: DL-based approaches can achieve high recognition accuracy by taking advantage of the network to store intelligence learned from mass data. However, the deep architecture induces severe computational complexity for online inference.
- 2) *Offline training overhead*: Another critical issue for DL-based approaches is the overhead of offline training phase, such as the training time and the necessity of mass training data, which consumes significant energy and severely hinders the implementation of DL-based approaches.
- 3) *Resource consumption of online retraining*: Only additive white Gaussian noise (AWGN) channel is assumed in the simulation of some previous works, which is good for the development stage, but not practical enough [29]-[31]. Besides, the real-world channels may vary over time which dramatically degrades the performance of DL-based approaches due to the mismatch between training data and inference data. Therefore, online retraining without intolerable resource consumption for channel adaptation is indispensable to ensure the model stays accurate.

In this paper, we aim to leverage the benefits of convolutional neural network for the problem of AMC. To address the three aforementioned issues, we present a novel approach for data transformation as shown in Fig. 1(b) and neural network-based channel estimator (NN-CE) with an efficient online retraining mechanism to overcome the time-varying fading channel as shown in Fig. 1(c).¹ The main contributions of this paper are summarized as follows:

- 1) *Accumulated polar feature for deep architecture*: We propose a novel technique to take advantage of human's domain knowledge to transform received signals into an easier classified domain, and it can help to improve the classification accuracy to near-optimal region. Besides, with the help of data transformation, the model size, training time, and training data can be significantly reduced, when compared with [31]. Thus, we dramatically reduce the computational complexity and lighten the training overhead by 99.8 times, which are more feasible for practical implementation and applications.
- 2) *Neural network-based channel estimator (NN-CE)*: We consider a fading channel with distorted amplitude and phase shift which leads to severe performance degradation in related works. Then, we design a neural network-based channel estimator to recover the distorted channel with 13% improvement at SNR = 0dB.

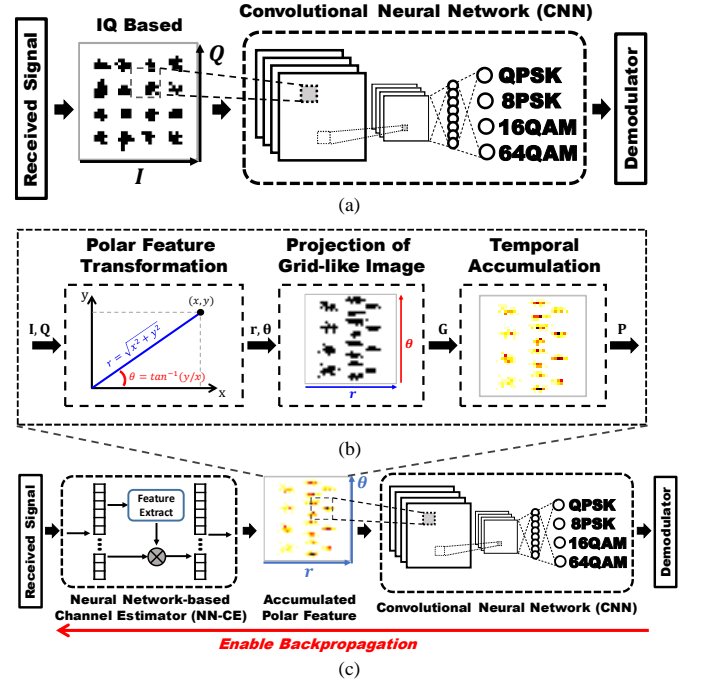


Fig. 1. Overview of (a) IQ based approach in [31], (b) proposed data transformation of accumulated polar feature, and (c) proposed accumulated polar feature based deep learning with neural network-based channel estimator.

- 3) *Efficient mechanisms for online retraining of NN-CE*: Considering the time-varying fading channel, we propose two efficient mechanisms for online retraining to remedy the degraded accuracy. With the benefit of NN-CE, we can reduce transmission overhead and retraining overhead by 90% and 76%, respectively. Therefore, the robustness under distorted channels can be effectively improved, which makes AMC practical in real-world applications.
- 4) Finally, we compare the computational complexity of proposed approach with prior arts to show that our approach can be more robust to fading channel under reasonable computational time. It can achieve higher recognition accuracy while using shorter inference time by 2,200 times compared with likelihood-based approach. Furthermore, the performance between different DL-based approaches is also evaluated on a public dataset for a fair comparison, which demonstrates the great efficiency of our method.

The comparison of related AMC frameworks is summarized in Table I. The rest of the paper is organized as follows. In Section II, the channel models and prior arts are introduced.

¹ <https://github.com/JieFangD/Automatic-Modulation-Classification>

The proposed deep learning architecture with data transformation is presented in Section III. In Section IV, the neural network-based channel estimator with the mechanisms of online retraining is introduced. Simulation results and analysis are conducted in Section V. The conclusions are finally drawn in Section VI.

II. CHANNEL MODEL AND REVIEW OF PRIOR ARTS

A. Notation

Throughout this paper, a normal-faced letter a denotes a scalar, a bold-faced lowercase letter \mathbf{a} denotes a vector, and a bold-faced uppercase letter \mathbf{A} denotes a matrix. Other operations used in this paper are defined as follows:

- $\mathbf{a}[p]$ means the p -th element of \mathbf{a} .
- $\mathbf{A}[p, :]$, $\mathbf{A}[:, q]$, and $\mathbf{A}[p, q]$ denote the p -th row vector, q -th column vector, and (p, q) -th entry of \mathbf{A} , respectively.
- \mathbf{A}^T denotes the transpose of \mathbf{A} .
- $|\cdot|$ denotes the element-wise absolute value or cardinality for a set.
- $[\mathbf{A}|\mathbf{B}]$ is the horizontal concatenation.

B. Channel Model

We assume that baseband in-phase (I) and quadrature (Q) components of $\mathbf{y}[n]$ are extracted in a coherent, synchronous environment with single-tone signaling. In our approach, channel is treated as a flat fading in which frequency and phase offsets are added separately. The baseband sample of $\mathbf{y}[n]$ after matched filtering can be expressed as:

$$\mathbf{y}[n] = a e^{j(2\pi f_0 n + \theta)} \mathbf{s}[n] + \mathbf{g}[n], \quad (1)$$

where a is an unknown amplitude factor, f_0 and θ are frequency offsets and unknown phase offsets, respectively, $\mathbf{s}[n]$ is transmitted symbol generated from one of selected modulations, and $\mathbf{g}[n]$ is the complex Gaussian noise. Therefore, the modulation classification task is to blindly identify these modulation categories merely from the N -sample received symbol vector $\mathbf{y} = [\mathbf{y}[0], \mathbf{y}[1], \dots, \mathbf{y}[N-1]]^T$.

In this paper, we firstly consider four different modulation types for the preliminary evaluation and analysis of proposed approaches, including QPSK, 8PSK, 16QAM, and 64QAM, which are motivated by their difficulty in modulation classification literatures and widely used in many standards. Finally, we evaluate the performance on a public RadioML2018.01a dataset with 24 different modulation types as depicted in Section VI.

C. Prior Art: Maximum Likelihood-based Approach [9]-[17]

Maximum likelihood-based (LB) approach can achieve optimal performance with Bayesian sense under ideal channel, such as additive white Gaussian channel, or perfect knowledge of channel parameters. Under AWGN channel, the probability of different modulation types can be easily derived as:

$$L(\mathbf{y}|m_i, \sigma) = \prod_{n=0}^{N-1} \sum_{k=1}^{M_i} \frac{1}{M_i} \frac{1}{\sqrt{2\pi}\sigma} e^{-\frac{|\mathbf{y}[n] - A_{i,k}|^2}{2\sigma^2}}, \quad (2)$$

$$m = \underset{m_i \in \mathcal{M}}{\operatorname{argmax}} L(\mathbf{y}|m_i, \sigma), \quad (3)$$

where m_i is the i th modulation type in modulation pool \mathcal{M} , σ is the variance of the signal-to-noise ratio, $A_{i,k}$ is the k th alphabet of the i th modulation, and $M_i = |\mathcal{A}_i|$ denotes the alphabet size of the i th modulation. The classified result m is based on the maximization of (2). Though LB methods have optimal performance, they suffer from high computational complexity for inference as well as high sensitivity to channel variation. Therefore, with the presence of fading channels, different likelihood ratio tests are proposed to overcome the problem of channel variation [9]-[17]. Among the different approaches, hybrid likelihood ratio test (HLRT) exploits a tradeoff between complexity and recognition accuracy. Then, (2) is revised as:

$$L_{HLRT}(\mathbf{y}|m_i, \sigma) = \max_{a_0 \in \alpha, \theta_0 \in \Theta} \prod_{n=0}^{N-1} \sum_{k=1}^{M_i} \frac{1}{M_i} \frac{1}{\sqrt{2\pi}\sigma} e^{-\frac{|\mathbf{y}[n] - a_0 e^{-j\theta_0} A_{i,k}|^2}{2\sigma^2}}, \quad (4)$$

where α and Θ are the set of unknown parameters of amplitude and phase, respectively. This method undergoes a long search process to find the unknown parameters which maximize the likelihood. The resolution of the set of the unknown parameters must be high enough to achieve better recognition accuracy. Therefore, the channel variation further increases the computational complexity of the LB methods. Finally, the analysis of complexity for different approaches will be compared and summarized in Section V.

D. Prior Art: Deep Learning-based Approach [27]-[36]

Recently, deep learning based approaches have been used to extract high-level features for AMC [27]-[36]. For example, one-dimensional convolutional neural network (CNN) is exploited in [28], [30], [32] and [36] to achieve promising performance with only raw IQ samples. Furthermore, [31] directly maps the received complex symbols to scatter points on the complex plane as the input for two-dimensional CNN which fully utilizes the characteristic of CNN with better performance as shown in Fig. 1(a). Although the method is simple and useful, learning from images in I - Q plane loses the domain knowledge and known characteristics of the communication systems. Besides, it is apparent that the constellation of QPSK can be seen as a sub-picture of 8PSK, which is called nested modulations as shown in Fig. 2(a). Likewise, 16QAM also has correlation with 64QAM. The shared constellation points in I - Q based images result in high misclassification between them and consume more resources for offline training. Therefore, in our previous work [33], we have demonstrated that learning features from polar coordinates can improve recognition accuracy as shown in Fig. 2(b), which was also exploited in [34] and [35] for one-dimensional CNN and long short-term memory (LSTM), respectively.

Another practical problem is that only AWGN channel was considered in the simulation of some prior arts, which is unrealistic and results in inevitable degradation of recognition accuracy under fading channel [29]-[31]. Besides, real-world channels may vary over time which lead to the mismatch

between training data and inference data, thus requiring the online retraining to make up for the dramatically degraded performance of DL-based approaches. Therefore, the resource consumption of online retraining, including transmission overhead and retraining overhead, needs to be carefully considered and addressed.

III. PROPOSED ACCUMULATED POLAR FEATURE BASED DEEP LEARNING ARCHITECTURE

Before applying the input data to the concatenated CNN model, we transform the received signal to an easier classified domain to reduce training overhead significantly. Also, the process of data transformation for accumulated polar feature can be mainly decomposed into three parts, polar feature transformation, projection of grid-like image, and temporal accumulation, as depicted in Fig. 1(b).

A. Construction of Grid-like Image in Polar Coordinates

1) *Polar Feature Transformation*: To deal with the aforementioned problem of resource consumption for offline training in $I - Q$ domain, we propose a polar feature transformation to map the complex symbols from Cartesian coordinates to polar coordinates. Learning features from $r - \theta$ domain encodes specific knowledge of the communication systems and makes the following convolutional neural network more robust to fading channel. Taking spectral analysis for example, we certainly can input time-series data into learning process. The training result might lead to a Fast Fourier Transform (FFT) with large noise term. However, if we apply existing expert domain know-how, data can be transformed with FFT during data preprocessing prior to training. Therefore, the polar feature transformation can reduce the part of feature extraction in neural networks with better performance and lower training overhead as shown in Section V.

In this paper, by leveraging existed expert knowledge in communication, we can transform $I - Q$ domain into $r - \theta$ domain before learning. To construct the relation between I and Q components, we associate with polar coordinates which replaces the $I - Q$ axis with $r - \theta$ axis, as illustrated in Fig. 2. The process of transformation is summarized in Algorithm 1, where \mathbf{I} , \mathbf{Q} represent real part and imaginary part of received complex symbols, \mathbf{r} , $\boldsymbol{\theta}$ represent the transformed polar coordinates of radius and theta, and N is the symbol length.

Algorithm 1: Polar Feature Transformation

Input \mathbf{I}, \mathbf{Q}

for $n = 0 : N - 1$ **do**

$$\mathbf{r}[n] \leftarrow \sqrt{\mathbf{I}[n]^2 + \mathbf{Q}[n]^2}$$

$$\boldsymbol{\theta}[n] \leftarrow \arctan(\mathbf{Q}[n]/(\mathbf{I}[n]))$$

end for

return $\mathbf{r}, \boldsymbol{\theta}$

2) *Projection of Grid-like Image*: To utilize 2D-CNN for classification, we need to project the transformed symbols in $r - \theta$ axis to grid-like images. The method is similar to [31]. However, they set the image resolution to 227×227 as the input setting of AlexNet model [37]. Considering the prohibitively high computational complexity and the demand of low latency

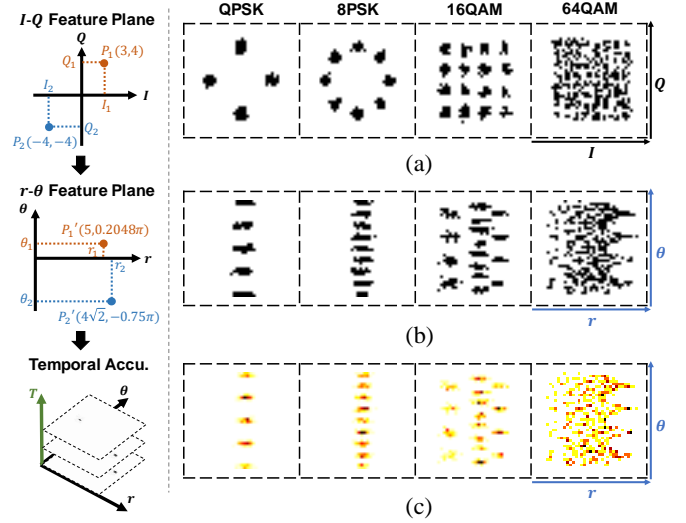


Fig. 2. Illustration of data transformation and constellation diagrams of four modulation categories with SNR=20dB: (a) $I - Q$ plane [31]; (b) $r - \theta$ plane [33]; (c) $r - \theta$ plane with temporal accumulation. (Note that darker color point represents higher values.)

Algorithm 2: Projection of Grid-like Image

Input $\mathbf{r}, \boldsymbol{\theta}, r_0, r_1, p_r, \theta_0, \theta_1, p_\theta$

Initialize Image Matrix $\mathbf{P} = \mathbf{0}$

Compute grid interval of r axis $\Delta g_r \leftarrow (r_1 - r_0)/p_r$

Compute grid interval of θ axis $\Delta g_\theta \leftarrow (\theta_1 - \theta_0)/p_\theta$

for $n = 0 : N - 1$ **do**

 Compute coordinate of r axis $i \leftarrow \lfloor (\mathbf{r}[n] - r_0)/\Delta g_r \rfloor$

 Compute coordinate of θ axis $j \leftarrow \lfloor (\boldsymbol{\theta}[n] - \theta_0)/\Delta g_\theta \rfloor$

if *polar_feature* **then**

 Compute pixel value of binary image $\mathbf{P}[i, j] \leftarrow 1$

else if *accumulated_polar_feature* **then**

 Compute pixel value of grayscale image

$$\mathbf{P}[i, j] \leftarrow \mathbf{P}[i, j] + 1$$

end if

end for

return \mathbf{P}

for communication, we design a specific convolutional model for the application of AMC and revise the image resolution from 227×227 to 36×36 , which result in great performance and dramatically reduce the computational overhead compared to AlexNet model.

The process of projection can be summarized in Algorithm 2, where r_0, r_1 are the range of radius axis, θ_0, θ_1 are the range of theta axis, p_r, p_θ are the image resolution of two axes. Firstly, we compute the grid interval of two axes, $\Delta g_r, \Delta g_\theta$ with regard to the input settings. Secondly, each transformed symbol in $r - \theta$ axis is mapped to one point on grid-like image with i, j representing the coordinate of r axis and θ axis, respectively. Finally, the pixel value of grid-like image \mathbf{P} is set to one, if there is any symbol mapped to the point. Therefore, we obtain the binary image, \mathbf{P} , with the value set to either zero or one. The polar feature based images of selected modulation categories are depicted in Fig. 2(b), where the horizontal and vertical axes represent radius and theta, respectively.

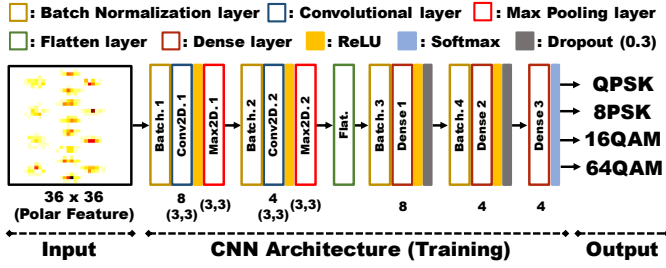


Fig. 3. The detailed architecture of designed convolutional neural network.

B. Temporal Accumulation

To further increase the classification accuracy, we add another temporal axis to accumulate historical information of symbols in this dimension, which is not considered in our previous work [33]. The schematic is shown in Fig. 2(c). Therefore, the grid-like image is converted from binary to colorful, and the different colors represent the different probabilities of a symbol appearance at that point. Though the additive white Gaussian noise can be considered as a random process and degrade the classification accuracy, the noised symbol still has a higher probability to appear near the original point. With this approach, the higher probability of appearance has darker color as shown in Fig. 2(c), which makes the classification easier. The projection process of accumulated polar feature is also depicted in Algorithm 2.

Finally, \mathbf{P} is the input data for the concatenated CNN model. In summary, with the polar feature transformation and temporal accumulation, we not only increase the classification accuracy but also reduce the size of neural network model and improve the convergence rate, which dramatically lower the offline training overhead of deep neural network as shown in Section V.

C. Convolutional Neural Network (CNN)

Deep learning (DL) is one of the fastest-growing fields with many breakthroughs recently. With different applications, there are many specifically customized architectures of neural networks. With that, convolutional neural network (CNN) is one of the widely adopt architectures in computer vision for object recognition and detection. A typical convolutional neural network architecture comprises of a number of convolutional layers for feature extraction, followed by fully connected layers (FC) for classification [37], [38].

The architecture of our CNN is constructed by two convolutional layers and three dense layers as illustrated in Fig. 3. The values below the convolutional layers represent the number and size of filters, and values below the dense layer represent the number of nodes. Before concatenating the next convolutional layer or dense layer, we add batch normalization layer to reduce training time and to avoid exploding or vanishing gradients [39]. More detailed descriptions of different layers can be found in [40]. The nonlinear activation function, Rectified Linear Unit (ReLU), among each layer is defined as:

$$\sigma_{ReLU}(x) = \max\{0, x\}. \quad (5)$$

Also, the activation function of softmax is to squash a K -dimensional input vector of arbitrary real values to K -dimensional vectors with each entry is in the range $(0,1]$ so that the summation of all entries is one. The softmax function is widely used in the output layer for classification to indicate the probability of each prediction. The function is defined as:

$$\sigma_{Softmax}(\mathbf{x}_j) = \frac{e^{x_j}}{\sum_{k=0}^{K-1} e^{x_k}}. \quad (6)$$

In addition, the regularization technique of “dropout”, which avoids updating the weights of part nodes, is also utilized to reduce overfitting and force the nodes be more independent than usual. Finally, the loss function \mathcal{L} , commonly categorical cross-entropy for classification tasks, is used to compute the error gradient between true labels \mathbf{y} and predict labels $\hat{\mathbf{y}}$ and can be defined as:

$$\mathcal{L}(\mathbf{y}, \hat{\mathbf{y}}) = -\frac{1}{K} \sum_{k=0}^{K-1} \mathbf{y}_k \log(\hat{\mathbf{y}}_k) + (1 - \mathbf{y}_k) \log(1 - \hat{\mathbf{y}}_k). \quad (7)$$

For the training process, we use Adadelta optimizer [41] and the technique of early stopping [42] is utilized to avoid overfitting and ensure the convergence of neural network weights based on the performance on a validation set.

IV. NEURAL NETWORK-BASED CHANNEL ESTIMATOR WITH ONLINE RETRAINING MECHANISM

In real-world wireless communications, there are many types of channel impairments, such as time dispersion, Doppler shifts, and inter-symbol interference. In this paper, we mainly focus on the impairments of fading channel, namely power scaling and phase shift, which result in severe degradation of classification accuracy. Besides, the channel impairments are time-varying that result in a serious problem for DL-based approaches, due to the mismatch between training data and inference data. To address the two issues mentioned above, we design a neural network-based channel estimator to eliminate the channel effect and revise our deep architecture to make the online retraining feasible and efficient.

A. Proposed Neural Network-based Channel Estimator (NN-CE)

Considering the channel impulse response, the received constellation map must be distorted in amplitude and phase, which makes the recovery of transmitted signal more challenging. Therefore, we design a neural network-based channel estimator to find out the inverse channel response and reduce the impact of power scaling and phase shift on the performance.

In [43], the team of Google DeepMind proposed a spatial transformer network to learn an appropriate transformation for the input picture. The spirit of [43] is to design a localization network to estimate the transformation parameters. This is particularly useful for the application of image recognition where the input images may suffer from warping, rotation, and scaling. With the spatial transformer network, the model can be more spatially invariant to the input data. Additionally, there are also some works adopting this concept to design their own

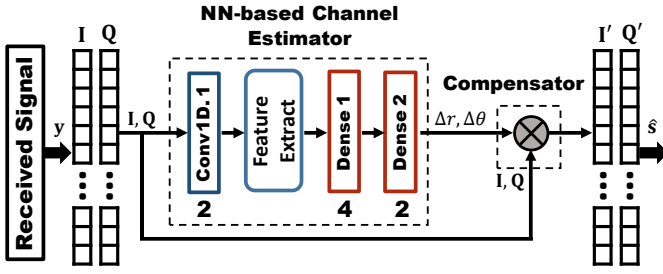


Fig. 4. The detailed architecture of neural network-based channel estimator (NN-CE) with two function-specific components: NN-based channel estimator and compensator.

networks in order to overcome common channel impairments, such as radio transformer network in [44], [45] and channel compensation network in our previous work [33].

In this part, we design a neural network-based channel estimator to deal with the problem of fading channel as depicted in Fig. 4. Compared to [33], we further take advantage of the domain knowledge of communication systems to constrain the hypothesis class of the proposed network to reduce model size and avoid overfitting. It can be mainly divided into two function-specific components. The first one, NN-based channel estimator, is to estimate the compensated parameters Δr and $\Delta \theta$. This can be achieved via some extracted features and the help of nonlinear transformation of neural networks. We firstly extract two features, average amplitude and standard deviation of the received signal, and feed them as the input for dense layers to transform the features to a higher level and estimate the compensated parameters. The second part, the compensator, takes the received signal as input and utilizes the estimated parameters to compensate for distorted signal. The process can be expressed as:

$$[I'|Q'] = [I|Q] \times \begin{bmatrix} \Delta r \cos(\Delta \theta) & -\Delta r \sin(\Delta \theta) \\ \Delta r \sin(\Delta \theta) & \Delta r \cos(\Delta \theta) \end{bmatrix}. \quad (8)$$

The model is very tiny with only 44 parameters and suitable for online retraining to adapt to time-varying fading channel without massive resource consumption. And this will be introduced in Section IV.B.

For the offline training, we can train NN-CE first and concatenate it to the proposed deep architecture in Section III as shown in Fig. 1(c). For the training data, the input and desired outputs are the received signal with channel distortion and transmitted signal without any channel effect, respectively. Therefore, the purpose of NN-CE is to recover the distorted signal. The loss function is the mean absolute error and can be given by:

$$\mathcal{L}(s_{golden}, \hat{s}) = \frac{1}{N} \sum_{n=0}^{N-1} |s_{golden}[n] - \hat{s}[n]|, \quad (9)$$

where s_{golden} is the transmitted signal and \hat{s} is the compensated signal from NN-CE. For the time invariant channel, we can train a model in an offline environment to fit the channel optimally. However, for real-world applications, the channel may vary over time and degrade the recognition accuracy.

B. Partial Retraining with Differentiable Transformation

To address the issue of time-varying channel, we need to retrain our model to maintain the high recognition accuracy.

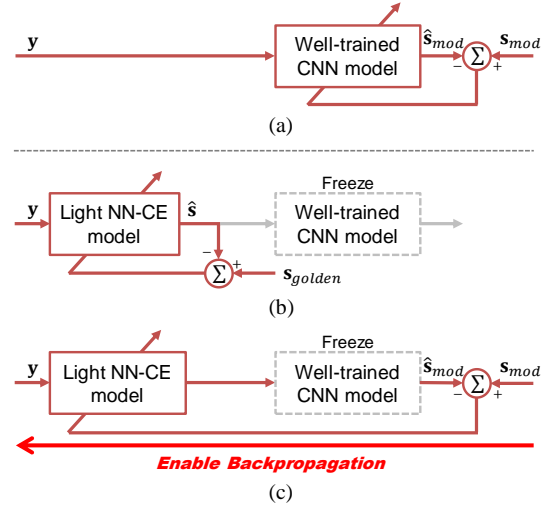


Fig. 5. Proposed mechanisms of online retraining: (a) retrain CNN without concatenation of NN-CE, (b) partially retrain NN-CE with s_{golden} , and (c) partially retrain NN-CE with s_{mod} via end-to-end optimization.

Besides, due to the fact that online retraining is resource-limited, efficient mechanism of retraining without intolerable resource consumption also needs to be carefully considered. Therefore, there are three different mechanisms of online retraining shown in Fig. 5 and we evaluate these mechanisms from two perspectives, namely in terms of transmission overhead and retraining overhead, which represent the occupied channel capacity for transmission of retraining data and the consumption of computing resource, respectively.

We first show that NN-CE can not only compensate for the distorted channel, but also make the online retraining more efficient. In Fig. 5(a), without the concatenation of light NN-CE model, we need to retrain the bigger CNN model with the labels of modulation types, which is also called s_{mod} . This method requires more retraining data to avoid overfitting, thus inducing severe transmission overhead and retraining overhead, according to the uniform convergence with no free lunch theorem [46]. Therefore, to avoid the massive resource consumption, another two mechanisms with NN-CE model are proposed and shown in Fig. 5(b) and Fig. 5(c), respectively. In Fig. 5(b), in order to partially retrain NN-CE, we set training sequence s_{golden} as the desired output. This method is efficient and effective in making up for the degradation with little retraining overhead. However, it induces huge transmission overhead due to the transmission of longer training sequence s_{golden} , which sacrifices the channel capacity and reduces the data throughput. Besides, the received signal y is only utilized in training phase without carrying any practical and effective information for communication.

To alleviate the transmission overhead, we propose another novel mechanism to partially retrain NN-CE without s_{golden} but with the label of modulation types s_{mod} as shown in Fig. 5(c). The main idea is to optimize the whole system in an end-to-end manner with partially updating the NN-CE model. With this approach, there are two issues that need to be solved: (i) connecting NN-CE with all transformation and the architecture of NN-CE to build up an integrated system, (ii) enabling the loss to back propagate from CNN to NN-CE with

Algorithm 3: Projection of Differentiable Grid-like Image

Input $\mathbf{r}, \theta, r_0, r_1, p_r, \theta_0, \theta_1, p_\theta$

Initialize Image Matrix $\mathbf{P} = \mathbf{0}$

Compute grid interval of r axis $\Delta g_r \leftarrow (r_1 - r_0)/p_r$

Compute grid interval of θ axis $\Delta g_\theta \leftarrow (\theta_1 - \theta_0)/p_\theta$

for $i = 0 : p_r - 1$ **do**

 Compute grid value of r axis $\mathbf{g}_r[i] \leftarrow r_0 + \Delta g_r \times i$

end for

for $j = 0 : p_\theta - 1$ **do**

 Compute grid value of θ axis $\mathbf{g}_\theta[j] \leftarrow \theta_0 + \Delta g_\theta \times j$

end for

for $n = 0 : N - 1$ **do**

for $i = 0 : p_r - 1$ **do**

for $j = 0 : p_\theta - 1$ **do**

$$\mathbf{P}[i, j] \leftarrow \mathbf{P}[i, j] + e^{-\frac{[(\mathbf{r}[n] - \mathbf{g}_r[i])^2 + (\theta[n] - \mathbf{g}_\theta[j])^2]}{(2\sigma^2)}}$$

end for

end for

end for

return \mathbf{P}

partially updating. However, the transformation proposed in Section III is not differentiable, which prohibits the gradients of loss to propagate through the whole system. To resolve this issue, we need to revise the Algorithm 2 in Section III to make the whole process differentiable. The non-differentiable function is mainly caused by the absolute value function, which is used in computing the coordinate of r axis and θ axis. Therefore, the Algorithm 2 is revised to prevent the usage of absolute value function as summarized in Algorithm 3.

With the replacement of differentiable Gaussian distribution, we successfully enable the back propagation from output to input and partially retrain NN-CE. The schematic of revised process of transformation and patterns are shown in Fig. 6(b). Compared with Fig. 6(a), the patterns are more smooth and can more accurately represent the occurrence probability of symbols on the picture.

Therefore, the shorter training sequence \mathbf{s}_{mod} can dramatically reduce the transmission overhead with only a little additional retraining overhead for the end-to-end optimization. Besides, the received signal \mathbf{y} can be used not only for the retraining of the model, but also for the transmission of practical information. For more detailed analysis of resource consumption, we compare the proposed mechanisms and evaluate the benefit of NN-CE in Section V.

V. SIMULATION RESULTS

In this section, we evaluate the performance of the proposed accumulated polar feature based approach with prior arts through several simulations. We compare the classification accuracy and computational complexity among the different approaches.

Each simulation result is obtained from Monte Carlo trials over 1,000 independent channel realizations for each signal modulation. The classification decision is drawn from the

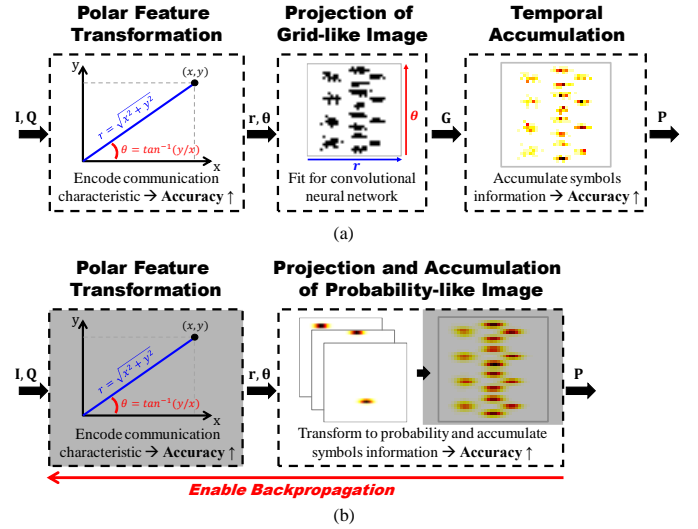


Fig. 6. Overview of (a) proposed data transformation of accumulated polar feature, and (b) revised transformation with enabled backpropagation.

TABLE II
SIMULATION SETTINGS

Parameters	Notation	Values
Modulation Pool	\mathcal{M}	QPSK, 8PSK, 16QAM, 64QAM
Training Data/Modulation	-	5000 images
Testing Data/Modulation	-	1000 images
Validation Ratio	-	0.2
Batch Size of Offline Training	-	100
Batch Size of Online Retraining	-	10
Image Resolution	p_r, p_θ	36
Range of Radius Axis	r_0, r_1	[0, 3]
Range of Theta Axis	θ_0, θ_1	$[-\pi/2, \pi/2]$
Amplitude Factor	a	$U(0.2, 1)$
Phase Offset	θ	$U(0, 2\pi)$
Variation Degree	δ	0.3, 0.5
Symbol Length	N	1000
Signal to Noise Ratio	SNR	-4, -2, 0, 2, 4, 6, 8, 10, 12
Training and Testing Environment	-	Deep learning library of Keras running on top of TensorFlow with i7-6700 CPU and NVIDIA GTX 1080 Ti GPU

modulation pool $\mathcal{M} = \{\text{QPSK}, \text{8PSK}, \text{16QAM}, \text{64QAM}\}$ as described in Section II.B. Therefore, the resulting classification accuracy is averaged over all 4,000 realizations. For the following experiments, if there is no specific statement, all parameters and environment settings are based on Table II.

A. Reduction of Offline Training Overhead

Before comparing against prior arts, we firstly define a metric for the evaluation of offline training overhead:

Offline Training Overhead

$$\triangleq (\text{Model Size}) \times (\# \text{ of Epoch}) \times (\# \text{ of Training Data})$$

With this defined metric, we compare the proposed accumulated polar feature based approach to [31] and [33] via

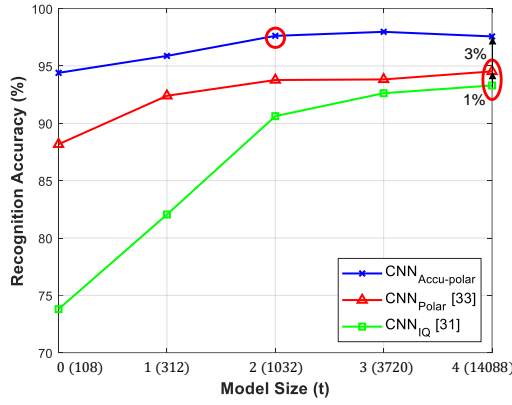


Fig. 7. Recognition accuracy against various model size when SNR = 8dB. Values beside model size represent the number of model parameters and red circle indicates the selected model size for different approaches.

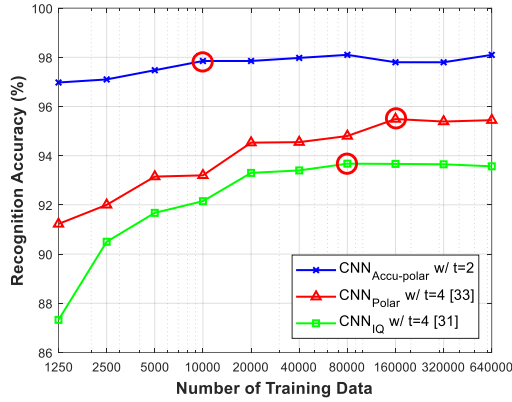


Fig. 8. Recognition accuracy against various number of training data when SNR = 8dB. Red circle indicates the selected number of training data for different approaches.

several experiments to evaluate the benefit of transformation described in Section III. Besides, for a fair comparison, the model architecture and image resolution for [31] and [33] are set as same as our approaches.

1) *Selection of Model Size*: Initially, we evaluate the performance under various model size with SNR = 8dB to depict the tradeoff between accuracy and offline training overhead and to decide the best model structure for us. Meanwhile, we evaluate the contributions of performance improvement from the techniques of polar feature transformation and temporal accumulation, respectively. Firstly, we fix the architecture of convolutional neural network as shown in Fig. 3. Besides, the number of filters for convolutional layer and nodes for dense layer are set to $\{Conv1, Conv2, Dense1, Dense2, Dense3\} = \{2^{t+1}, 2^t, 2^{t+1}, 2^t, 4\}$, where t varies from 0 to 4. In Fig. 7, we can first see that with the polar feature transformation, the signal is encoded to an easier classified domain with 1% improvement when $t = 4$. Next, the temporal accumulation can further enhance the performance by 3% with the accumulated historical information. For the following comparison, to highlight the tradeoff between performance and offline training overhead, the model size for IQ-based, polar-based, and accumulated polar-based are set to 4, 4, and 2, respectively. We can observe that our proposed transformation can effectively reduce model size and enhance performance.

TABLE III
RUN TIME OF TRAINING PHASE

	IQ [31]	Polar [33]	Accu-polar
Model Size (t)	4	4	2
Time per Epoch (s)	1.64	1.64	1.08
Number of Epoch	23.22	16.89	16.78
Training Time (s)	38.08 (2.1×)	27.70 (1.5×)	18.12 (1×)

TABLE IV
OFFLINE TRAINING OVERHEAD OF DIFFERENT DL-BASED APPROACHES

	IQ [31]	Polar [33]	Accu-polar
Model Size (t) / Model Parameter	4 / 14,088	4 / 14,088	2 / 1,032
Number of Training Data	80,000	160,000	10,000
Accuracy	93.5	95.5	97.9
Time per Epoch (s)	4.40	8.07	1.08
Number of Epoch	15.33	14.67	16.78
Training Overhead	17,277,523k (99.8×)	33,067,353k (190.9×)	173,169k (1×)

2) *Convergence Rate*: The most challenging issue for DL-based approaches is the training phase, which requires a lengthy period of time and considerable energy, has caused huge barriers of implementation for many years. Therefore, the training time for different deep learning based approaches are compared in Table III. We can observe that the transformation of data prior to training can speed up the convergence rate by 2.1 times which means that we can transform signals to an easier classified domain to reduce training time. The detailed complexity analysis of the proposed method and prior arts are analyzed and compared in Section V.E, including the operation of data transformation.

3) *Number of Training Data*: Another important issue for DL-based approaches is the number of training data. Labeled training data for practical applications is very precious and rare, usually requiring great amounts of resources to obtain. In Fig. 8, we show that our proposed accumulated polar feature can converge with merely 10,000 training data. On the other hand, IQ-based and polar-based approaches require 80,000 and 160,000 training data for convergence, respectively. Furthermore, with a relatively low volume of training data, the proposed approach achieves a significant performance improvement, which proves the importance of data transformation and the domain knowledge that are helpful in reducing the required number of training data, by transforming data to an easier classified domain.

To sum up, a comprehensive comparison with evaluation metrics is shown in Table IV. We can observe that the data transformation significantly reduces the offline training overhead by about 100 times and 190 times compared to [31] and [33], respectively, and has better efficiency and accuracy.

B. Performance under Various Conditions

1) *Various SNR values under AWGN Channel*: With the chosen model size, we compare our proposed approach to prior arts under various SNR. In Fig. 9, we can observe that the LB method [13] can achieve optimal performance in Bayesian

sense under AWGN channel. Therefore, we can treat [13] as the upper bound for the recognition accuracy. Simultaneously, we compare the performance to high-order cumulants (HOCs) with fourth order (C_{40}, C_{42}) and sixth order (C_{63}), which are detailed explained in [9]-[12], [18]-[23]. From the simulation results, our proposed method is far better than FB method [21] by 25.4% when $\text{SNR} = 0\text{dB}$, and is very close to the upper bound under high SNR conditions. Besides, our proposed accumulated polar feature is about 3% better than IQ-based approach [31] under the whole range of SNR values with a smaller model size.

2) *Various Symbol Lengths under AWGN Channel*: In Fig. 10, we compare the different approaches against various symbol lengths when $\text{SNR} = 8\text{dB}$. With a longer length, all approaches achieve better performance, as expected. We observe that our approach is still the closest to the upper bound under different symbol lengths. Therefore, our approach has the high flexibility to meet different requirements under various symbol lengths, such as low latency for shorter packets and high accuracy for longer packets. Due to the poor performance of FB, we do not make comparison to it in the following experiments.

3) *Various SNR values under Fading Channel*: To make the system more practical, we consider the fading channel with variance of received power and phase shift that is a common phenomenon in communication systems. The setup of variances α and θ are shown in Table II, and other settings are kept the same as given in the previous experiment. Besides, we also evaluate the performance of the proposed approach with NN-CE, which has the ability to learn the inverse channel response and compensate for the distorted channel. The simulation results are shown in Fig. 11. When considering the fading channel, the performance degrades significantly, especially for the LB method which suffers from channel mismatch. Despite adopting HLRT method described in [15], it still experiences severe performance degradation under fading channels. As a tradeoff between the complexity and recognition accuracy, the spacing of unknown parameters of amplitude and phase for HLRT are set to 0.05 and 1, respectively. In contrast, our proposed accumulated polar feature outperforms all other methods by more than 16% under most range of SNR, which demonstrates that our method is robust and tolerant to the channel distortion. Besides, the NN-CE can compensate for the channel distortion, which further improves the recognition accuracy by 13% when $\text{SNR} = 0\text{dB}$ under a practical environment and approaches the upper bound of ideal channel under high SNR conditions.

C. Performance under Time-varying Fading Channel with Different Mechanisms of Online Retraining

Since channels may vary over time in real-world environments, we need online retraining to maintain the high recognition accuracy. NN-CE can not only compensate for the channel distortion, but also provide an efficient way for online retraining. In this part, we evaluate the proposed mechanisms of online retraining under different degrees of channel variation with varying sizes of retraining data. We first randomly generate an independent channel as the current channel

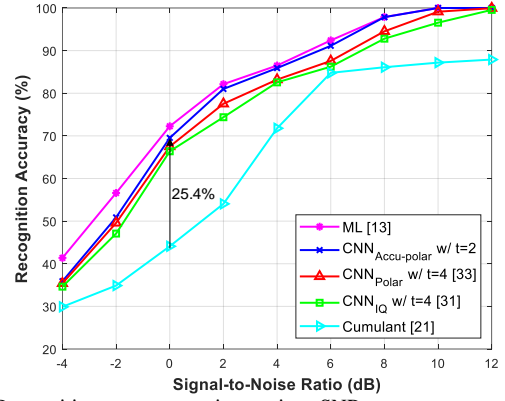


Fig. 9. Recognition accuracy against various SNR.

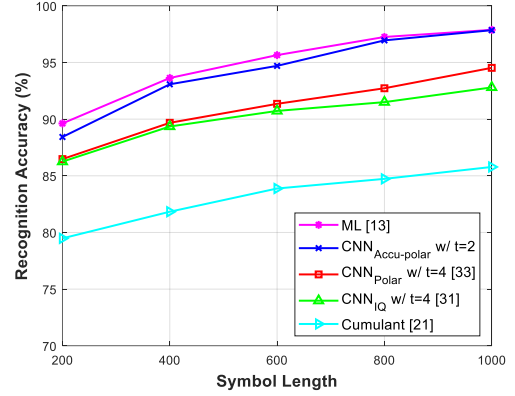


Fig. 10. Recognition accuracy against various symbol lengths.

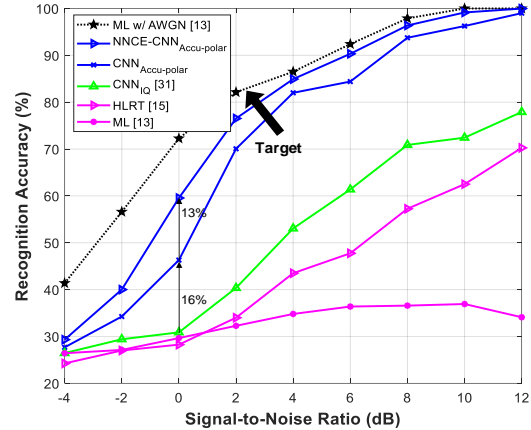


Fig. 11. Recognition accuracy against various SNR under fading channel.

according to the distribution listed in Table II and the model is well-trained under this setting. To model the effects of a time-varying channel, the amplitude factor and phase offset change according to the setting of variation degree, namely the parameters of fading channel will become $\alpha' = \alpha \times (1 \pm \delta)$ and $\theta' = \theta \times (1 \pm \delta)$ where the positive and negative signs are randomly decided. Therefore, the time-varying channel severely degrades the recognition accuracy due to the mismatch between training data and inference data. By the following reason, online retraining is required to make up for the degraded performance.

1) *Time-varying Fading Channel without NN-CE*: Firstly, we evaluate the proposed accumulated polar feature without the

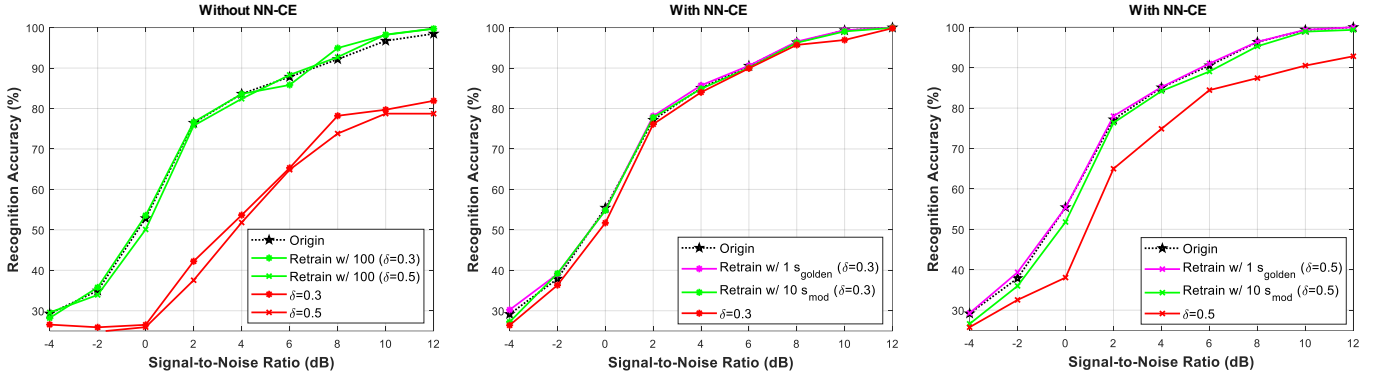


Fig. 12. Recognition accuracy of online retraining under time-varying fading channel: (a) online retraining without NN-CE, (b) proposed mechanisms of online retraining with $\delta = 0.3$, and (c) proposed mechanisms of online retraining with $\delta = 0.5$.

help of NN-CE, which means that the model is more sensitive to channel variation and require more retraining data to avoid overfitting. In Fig. 12(a), each point is the average of 4000 realizations under five different channels. We show that the performance degrades dramatically under 0.3 or 0.5 channel variation, and at least 100 data cases of each type of modulation are required to retrain the model back to original performance. Though the required retraining data is less than training data, it still sacrifices the channel capacity for the transmission of retraining data and requires massive computing resource for the process of retraining.

2) *Time-varying Fading Channel with NN-CE*: With the benefits from NN-CE, two different mechanisms of online retraining, partial retraining NN-CE with \mathbf{s}_{golden} and end-to-end optimization with \mathbf{s}_{mod} , have been detailed in Section IV.B. First, from Fig. 12(b) and Fig. 12(c), we can observe that the degradation is less compared to Fig. 12(a), which means that NN-CE can make our system more robust to channel variation. Second, with the label of training sequence \mathbf{s}_{golden} , we can effectively retrain our system back to original performance with only 1 data case for each type of modulation, consuming very little computing resources. However, the required long training sequence still induces severe transmission overhead. On the other hand, though the approach of end-to-end optimization requires 10 labeled data samples specifying the modulation types \mathbf{s}_{mod} for each type of modulation, the transmitted data can be used not only for retraining the model, but also for the transmission of practical information, which dramatically reduces the transmission overhead with minimal additional retraining overhead.

D. Analysis of Online Retraining

In this part, we further evaluate the resource consumption of different mechanisms of online retraining from two perspectives, transmission overhead and retraining overhead, which represent the occupied channel capacity for transmission of retraining data and consumption of computing resources, respectively. The two metrics can be given by:

$$\text{Transmission Overhead} \triangleq \text{Occupied Channel Capacity} \\ = (\# \text{ of Retraining Data}) \times (\text{Length per Data}),$$

and

$$\text{Retraining Overhead} \triangleq \text{Retraining Time}.$$

TABLE V
RESOURCE CONSUMPTION OF DIFFERENT MECHANISMS OF ONLINE RETRAINING

	Retrain CNN w/o NN-CE	Partially Retrain NN-CE	
Label	\mathbf{s}_{mod}	\mathbf{s}_{golden}	\mathbf{s}_{mod}
Length per Data (bit)	$\log_2 M = 2$	$2N = 2000$	$\log_2 M = 2$
Number of Retraining Data	400	4	40
Transmission Overhead (bit)	800 (1 \times)	8000 (10 \times)	80 (0.1 \times)
Retraining Overhead (s)	11.24 (1 \times)	0.64 (0.057 \times)	2.67 (0.238 \times)

Table V lists the transmission overhead and retraining overhead of three different mechanisms of online retraining as shown in Fig. 5. The required data length of \mathbf{s}_{mod} is $\log_2 M$, representing the different types of modulations. On the other hand, \mathbf{s}_{golden} must be the same length as the symbol length of \mathbf{y} for the retraining of NN-CE. Furthermore, \mathbf{y} also needs to be accounted as retraining data because it is only utilized in the training phase without any actual information.

Firstly, it can be seen that without the help of NN-CE, it suffers from dramatic transmission overhead and retraining overhead. Secondly, when \mathbf{s}_{golden} is adopted as the label, retraining overhead can be reduced by 94% due to the benefit from the light NN-CE model. However, the data length of \mathbf{s}_{golden} induces severe transmission overhead. Finally, the mechanism of end-to-end optimization can successfully reduce dramatic transmission overhead and retraining overhead by 90% and 76%, respectively. Therefore, we can adjust between these two efficient mechanisms for online retraining based on different requirements.

E. Analysis of Computational Complexity

To evaluate the computational complexity, the number of different operations required by different classifiers and their corresponding inference time on a CPU are calculated and listed in Table VI. In this part, we also consider the operations of transformation. The analysis is based on a signal with length N among M potential modulation candidates. M_i denotes the alphabet size of the i th modulation candidate; $N_a = |\alpha|$ and $N_\theta = |\Theta|$ represent the size of the set of unknown parameters for HLRT.

TABLE VI
NUMBER OF OPERATORS AND OPERATION TIME REQUIRED BY DIFFERENT CLASSIFIERS

Channel	Classifier	Additions	Multiplications	Exponentials	Logarithms	Comparisons	Memory	Inference Time with CPU (s)
AWGN	ML [13]	$N(4\sum_{i=1}^M M_i + M) \sim 10^5$	$N(7\sum_{i=1}^M M_i + 4) \sim 10^6$	$N\sum_{i=1}^M M_i \sim 10^5$	$NM \sim 10^3$	$M = 4$	$\sum_{i=1}^M M_i = 92$	0.00972
	Cumulant [21]	$6N \sim 10^4$	$16N \sim 10^4$	0	0	$M = 4$	$3M = 12$	0.00036
	IQ [31]	$809p_r p_\theta + M + 2N \sim 10^6$	$809p_r p_\theta + M + 3N \sim 10^6$	$M = 4$	0	$116p_r p_\theta + N \sim 10^5$	$14020 + 17M = 14088$	0.00132
	Accu-polar	$p_r p_\theta (4N + 107) + M \sim 10^7$	$p_r p_\theta (6N + 106) + M \sim 10^7$	$p_r p_\theta N + M \sim 10^6$	0	$29p_r p_\theta \sim 10^4$	$1012 + 5M = 1032$	0.00773
Fading	HLRT [15]	$N_a N_\theta N(4\sum_{i=1}^M M_i + M) \sim 10^9$	$N_a N_\theta N(9\sum_{i=1}^M M_i) \sim 10^9$	$2N_a N_\theta N\sum_{i=1}^M M_i \sim 10^8$	$N_a N_\theta NM \sim 10^6$	$N_a N_\theta M \sim 10^3$	$\sum_{i=1}^M M_i = 92$	17.11982
	Accu-polar with NN-CE	$p_r p_\theta (4N + 107) + M \sim 10^7$	$p_r p_\theta (6N + 106) + M \sim 10^7$	$p_r p_\theta N + M \sim 10^6$	0	$29p_r p_\theta \sim 10^4$	$1056 + 5M = 1076$	0.00775

From Table VI, we can observe that cumulant [21] has the lowest complexity and inference time, but with the worst performance. Though ML [13] has optimal performance under AWGN channel, it is sensitive to channel mismatch and not practical for implementation. Therefore, DL-based approaches exploit the tradeoff between LB and FB approaches at the cost of memory usage. Besides, under the fading channel, the overhead of NN-CE is small enough with only a small increase in inference time, which is far less than HLRT [15], by 2200 times with significant improvement. Another interesting observation is that although our proposed approach has smaller model size, it has a higher inference time than IQ-based [31]. This is due to the extra operations of exponential function in Algorithm 3.

Besides, the computational complexity of LB approaches increases rapidly with the number of potential modulation candidates M , in the scale of $\mathcal{O}(N)$ and $\mathcal{O}(N_a N_\theta N)$ which are not scalable. However, the proposed method is in the scale of $\mathcal{O}(1)$, meaning that we can support more modulation candidates without growth in computational complexity.

F. Performance Evaluation on RadioML Dataset

Finally, we evaluate the proposed accumulated polar-based approach on a publicly available dataset as a benchmark for a fair comparison. Besides, we also compare our approaches with prior arts of neural network-based classifiers, including one-dimensional CNN [28], IQ-based CNN [31], residual network (ResNet) [32], and LSTM [35]. Compared to earlier released RadioML2016.10a, the used RadioML2018.01a dataset in this work is much more difficult, which has 24 different modulations and was firstly evaluated in [32]. The dataset is synthetically generated using GNU Radio with a number of realistic channel imperfections, such as multipath fading, channel frequency offset, and sample rate offset [47].

In this dataset, it contains 24 digital and analog modulation types with SNR ranging from -20 dB to 30 dB and the space is 2 dB. For each modulation type at each SNR value, there are 4096 examples with a length of 1024. Thus, there are about 2.5 million examples in total. However, due to the poor performance below -10 dB and no improvement over 20 dB, we only utilize the data with SNR between -10 dB and 20 dB. The dataset parameters are summarized in Table VII. For more details about this dataset, please refer to [32] and [47].

TABLE VII
RADIOML2018.01A DATASET PARAMETERS

Modulation Types	OOK, 4ASK, 8ASK, BPSK, QPSK, 8PSK, 16PSK, 32PSK, 16APSK, 32APSK, 64APSK, 128APSK, 16QAM, 32QAM, 64QAM, 128QAM, 256QAM, AM-SSB-WC, AM-SSB-SC, AM-DSB-WC, AM-DSB-SC, FM, GMSK, OQPSK
Sample Length	1024
SNR Range	-10, -8, -6, -4, -2, 0, 2, 4, 6, 8, 10, 12, 14, 16, 18, 20
Number of Training Data	707,712
Number of Validation Data	78,720
Number of Testing Data	786,432

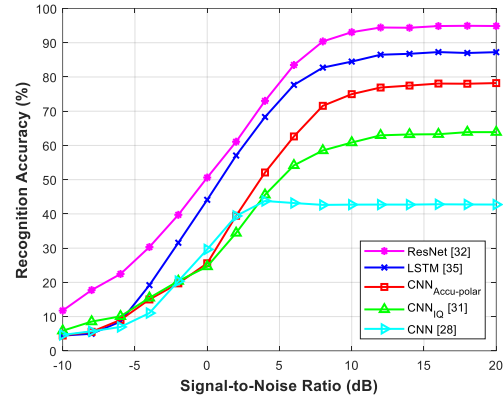


Fig. 13. Recognition accuracy against various SNR on RadioML dataset.

Firstly, we compare our proposed approach to prior arts under various SNR. Notice that the part of NN-CE is not included in this experiments and the model size t for both IQ-based CNN [31] and the proposed accumulated polar feature is increased to 32 due to this dataset is more difficult than our previous simulation settings. For the other prior arts, we implement the classifiers based on the proposed model architecture. In Fig. 13, we can observe that ResNet [32] can achieve best performance and LSTM [35] also outperforms our proposed approach under such a big dataset. However, without enough training data, these two methods will degrade and are worse than our approach, which is not shown in this paper.

Furthermore, we compare the model size and training time between these approaches as shown in Table VIII. From Table VIII, we can observe that LSTM consumes about 100 times memory overhead and 20 times training time compared to our

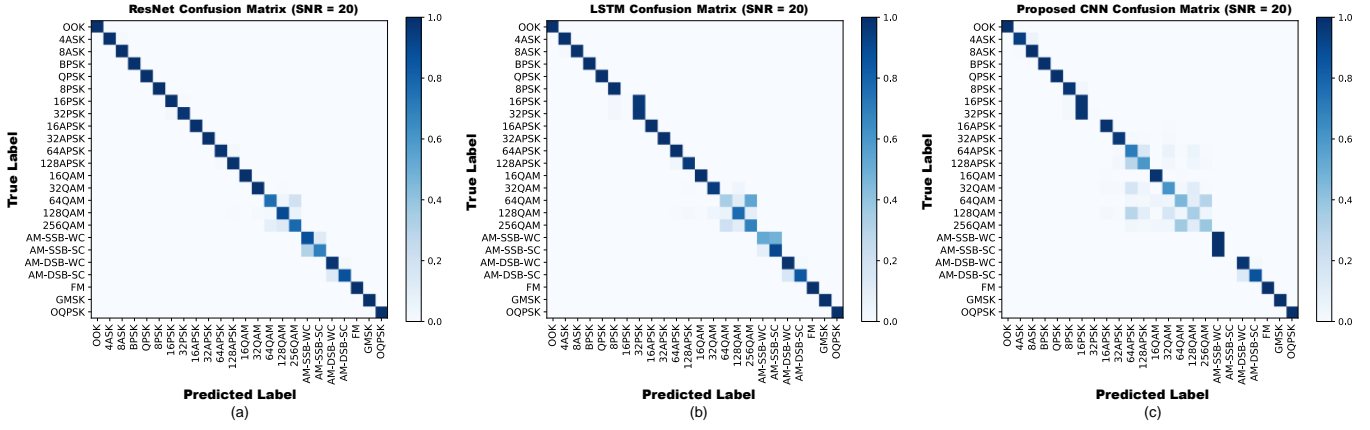


Fig. 14. Confusion matrix of different neural network-based classifiers on RadioML dataset at 20 dB: (a) ResNet [32], (b) LSTM [35], and (c) proposed approach.

approach, which is intolerable for real applications. On the other hand, though ResNet can avoid significant memory overhead via max pooling layer, its computational complexity is still too high to implement in communication systems.

Then, the confusion matrix of ResNet, LSTM, and the proposed method are shown in Fig. 14 for the analysis of classification accuracy between different modulation types. From Fig. 14, we can observe that ResNet has the cleanest diagonal in the confusion matrix due to its superior classification accuracy. On the other hand, for both LSTM and the proposed method, we can observe that there is serious misclassification appearing between high-order modulation types and AM modes, such as PSK, QAM, with-carrier (WC), and suppressed-carrier (SC), due to the similar symbol structure as concluded in [32].

In summary, though the recognition accuracy of our proposed method is worse than [32] and [35] on this dataset, the model size and computational complexity are far smaller, which is more feasible for practical implementation and applications. Moreover, for further improvement of recognition accuracy, we provide two directions as future works. Firstly, the NN-CE can be utilized with dedicated design to compensate for the channel impairments, which makes the signal easier classified and thus avoids complicated and powerful neural networks for classification. Secondly, inspired by [36], the proposed approach can be used in the first stage for fast and efficient classification and the indistinguishable modulation types, such as high-order PSK and AM-SSB in Fig. 14, can be further classified in the second stage with a more powerful classifier, which can improve both accuracy and system efficiency.

VI. CONCLUSION

In this paper, a novel accumulated polar feature based deep learning with channel compensation mechanism for AMC is presented. First, with the accumulated polar feature, it can learn from r - θ domain with historical information to reduce the offline training overhead and approach optimal recognition accuracy. Second, the proposed NN-CE can compensate for the distorted signal in realistic channel. Moreover, we propose two mechanisms for online retraining to deal with the time-varying fading channel; while having lower transmission overhead and

TABLE VIII
COMPARISON OF MODEL SIZE AND TRAINING TIME BETWEEN PROPOSED METHOD AND PRIOR ARTS

Models	ResNet [32]	LSTM [35]	Proposed Approach	IQ [31]	CNN [28]
Accuracy @ 20 dB	94.9	87.2	78.2	63.9	42.7
Model Parameters	238,840 (4.3×)	5,442,900 (98.2×)	55,452 (1×)	55,452 (1×)	1,319,200 (23.8×)
Time per Epoch (s)	124	950	20	20	44
Number of Epoch	71	32	73	63	109
Total Training Time (s)	8,804 (6.03×)	30,400 (20.82×)	1,460 (1×)	1,260 (0.86×)	4,796 (3.28×)

retraining overhead. Therefore, the proposed design can be used as an enabling technique for realizing intelligent receiver in realistic environments. For future extensions, we may consider real channels in future IoT and V2X applications.

REFERENCES

- [1] 3GPP R1-162195, *Qualcomm Inc.*, “mMTC KPI evaluation assumptions,” April 2016.
- [2] Dave Evans, “The Internet of Things: How the Next Evolution of the Internet Is Changing Everything,” Cisco Internet Business Solutions Group (IBSG), Cisco Systems, Inc., San Jose, CA, USA, White Paper 2011.
- [3] Friedrich K. Jondral, “Software-defined radio: basics and evolution to cognitive radio,” *EURASIP Journal on wireless communications and networking* 2005.3 (2005): 275-283.
- [4] K. E. Nolan, L. Doyle, P. Mackenzie, and D. O'Mahony, “Modulation scheme classification for 4G software radio wireless networks,” *Proc. IASTED*, 2002.
- [5] Simon Haykin, “Cognitive radio: brain-empowered wireless communications,” *IEEE Journal on Selected Areas in Communications* 23.2 (2005): 201-220.
- [6] H. Sun, A. Nallanathan, C.-X. Wang, and Y. Chen, “Wideband spectrum sensing for cognitive radio networks: A survey,” *IEEE Wireless Commun.*, vol. 20, no. 2, pp. 74-81, Apr. 2013.
- [7] P. Rawat, K. D. Singh, and J. M. Bonnin, “Cognitive Radio for M2M and Internet of Things: A Survey,” *Computer Commun.*, vol. 94, 2016, pp. 1–29.
- [8] A. A. Khan, M. H. Rehmani, and A. Rachedi, “Cognitive-radio-based Internet of Things: Applications architectures spectrum related functionalities and future research directions,” *IEEE Wireless Commun.*, vol. 24, no. 3, pp. 17-25, Jun. 2017.
- [9] O. A. Dobre, A. Abdi, Y. Bar-Ness, and W. Su, “Blind modulation classification: a concept whose time has come,” in *Proc. IEEE Sarnoff Symposium*, 2005, pp. 223-228.

- [10] O. A. Dobre, A. Abdi, Y. Bar-Ness, and W. Su, "Survey of automatic modulation classification techniques: Classical approaches and new trends," *IET Commun.*, vol. 1, no. 2, pp. 137-156, April 2007.
- [11] O. A. Dobre, "Signal identification for emerging intelligent radios: Classical problems and new challenges," *IEEE Instrum. Meas. Mag.*, vol. 18, no. 2, pp. 11-18, Apr. 2015.
- [12] Z. Zhu and A. K. Nandi, *Automatic Modulation Classification: Principles, Algorithms and Applications*. London: Wiley, 2015.
- [13] J. A. Sills, "Maximum-likelihood modulation classification for PSK/QAM," in *Proc. IEEE MILCOM*, Atlantic City, NJ, Oct. 31-Nov. 3 1999.
- [14] W. Wei, and J. M. Mendel, "Maximum-likelihood classification for digital amplitude-phase modulations," *IEEE Trans. Commun.*, 2000, 48, pp. 189-193.
- [15] P. Panagiotou, A. Anastasopoulos, and A. Polydoros, "Likelihood ratio tests for modulation classification," *Proc. IEEE MILCOM*, pp. 670-674, 22-25 Oct 2000.
- [16] A. Abdi, O. A. Dobre, R. Choudhry, Y. Bar-Ness, and W. Su, "Modulation classification in fading channels using antenna arrays," in *Proc. IEEE MILCOM*, vol. 1, Nov. 2004, pp. 211-217.
- [17] J. L. Xu, W. Su, and M. C. Zhou, "Likelihood ratio approaches to automatic modulation classification," *IEEE Trans. Systems Man and Cybernetics: Part C*, vol. 41, pp. 455-469, July 2011.
- [18] A. Swami and B. M. Sadler, "Hierarchical digital modulation classification using cumulants," *IEEE Trans. Commun.*, vol. 48, no. 3, pp. 416-429, 2000.
- [19] O. A. Dobre, Y. Bar-Ness, and W. Su, "Higher-order cyclic cumulants for high order modulation classification," in *Proc. IEEE MILCOM*, vol. 1, Oct. 2003, pp. 112-117.
- [20] H. Wu, M. Saquib, and Z. Yun, "Novel automatic modulation classification using cumulant features for communications via multipath channels," *IEEE Trans. Wireless Commun.*, vol. 7, pp. 3098-3105, 2008.
- [21] V. D. Orlic and M. L. Dukic, "Automatic modulation classification algorithm using higher-order cumulants under real-world channel conditions," *IEEE Commun. Lett.*, vol. 13, no. 12, pp. 917-919, Dec. 2009.
- [22] O. A. Dobre, Y. Bar-Ness and W. Su, "Cyclostationarity-based modulation classification of linear digital modulations in flat fading channels," *Springer Wireless Personal Communications*, 2009.
- [23] O. A. Dobre, M. Oner, S. Rajan, and R. Inkol, "Cyclostationarity-based robust algorithms for QAM signal identification," *IEEE Commun. Lett.*, vol. 16, no. 1, pp. 12-15, Jan. 2012.
- [24] Cheol-Sun Park, Won Jang, Sun-Phil Nah, and Dae Young Kim, "Automatic Modulation Recognition using Support Vector Machine in Software Radio Applications," in *Proc. 9th IEEE ICACT*, Feb. 2007, pp. 9-12.
- [25] X. Zhou, Y. Wu, and B. Yang, "Signal classification method based on support vector machine and high-order cumulants," *Wireless Sens. Netw.*, vol. 2, no. 1, pp. 48-52, 2010.
- [26] M. W. Aslam, Z. Zhu, and A. K. Nandi, "Automatic Modulation Classification using Combination of Genetic Programming and KNN," *IEEE Trans. Wireless Commun.*, vol. 11, no. 8, pp. 2742-2750, Aug. 2012.
- [27] B. Kim, J. Kim, H. Chae, D. Yoon, and J. W. Choi, "Deep neural network-based automatic modulation classification technique," in *International Conference on Information and Communication Technology Convergence (ICTC)*, Oct 2016, pp. 579-582.
- [28] T. J. O'Shea, J. Corgan, and T. C. Clancy, "Convolutional radio modulation recognition networks," in *Proc. Int. Conf. Eng. Appl. Neural Netw.*, pp. 213-226, 2016.
- [29] G. J. Mendis, J. Wei, A. Madanayake, "Deep learning-based automated modulation classification for cognitive radio," in *Proc. IEEE Int. Conf. Commun. Syst. (ICCS)*, Dec. 2016, pp. 1-6.
- [30] N. E. West and T. J. O'Shea, "Deep architectures for modulation recognition," in *Proc. 2017 IEEE Int. Symposium Dynamic Spectrum Access Networks (DySPAN)*, March 2017, pp. 1-6.
- [31] S. Peng, H. Jiang, H. Wang, H. Alwageed, and Y.-D. Yao, "Modulation classification using convolutional Neural Network based deep learning model," in *Proc. 26th Wireless Opt. Commun. Conf. (WOCC)*, Newark, NJ, USA, 2017, pp. 1-5.
- [32] T. J. O'Shea, T. Roy, and T. C. Clancy, "Over-the-Air Deep Learning Based Radio Signal Classification," *IEEE J. Sel. Topics Signal Process.*, vol. 12, no. 1, pp. 168-179, Feb. 2018.
- [33] C. F. Teng, C. C. Liao, C. H. Chen, A. Y. Wu, "Polar Feature based Deep Architecture for Automatic Modulation Classification Considering Channel Fading," in *Proc. 2018 IEEE Global Conference on Signal and Information Processing (GlobalSIP)*, Nov. 2018, pp. 554-558.
- [34] M. Kulin, T. Kazaz, I. Moerman, and E. D. Poorter, "End-to-End Learning from Spectrum Data: A Deep Learning Approach for Wireless Signal Identification in Spectrum Monitoring Applications," *IEEE Access*, vol. 6, pp. 18484-18501, 2018.
- [35] S. Rajendran, W. Meert, D. Giustiniano, V. Lenders, and S. Pollin, "Deep Learning Models for Wireless Signal Classification with Distributed Low-Cost Spectrum Sensors," *IEEE Trans. Cogn. Commun. Netw.*, vol. 4, no. 3, pp. 433-445, Sep. 2018.
- [36] Y. Wang, M. Liu, J. Yang and G. Gui, "Data-Driven Deep Learning for Automatic Modulation Recognition in Cognitive Radios," *IEEE Transactions on Vehicular Technology*, vol. 68, no. 4, pp. 4074-4077, April 2019.
- [37] A. Krizhevsky, I. Sutskever, and G. E. Hinton, "ImageNet classification with deep convolutional neural networks," in *Proc. Adv. Neural Inf. Process. Syst.*, 2012, pp. 1097-1105.
- [38] Y. LeCun, L. Bottou, Y. Bengio, and P. Haffner, "Gradient-based learning applied to document recognition," *Proc. IEEE*, vol. 86, no. 11, pp. 2278-2324, Nov. 1998.
- [39] S. Ioffe and C. Szegedy, "Batch normalization: Accelerating deep network training by reducing internal covariate shift," in *Proc. Int. Conf. Mach. Learn.*, 2015, pp. 448-456.
- [40] I. Goodfellow, Y. Bengio, and A. Courville, *Deep Learning*. Cambridge, MA, USA: MIT Press, 2016.
- [41] M. D. Zeiler, "ADADELTA: An adaptive learning rate method," *arXiv preprint arXiv:1212.5701*, 2012.
- [42] Y. Yao, L. Rosasco, A. Caponnetto, "On early stopping in gradient descent learning," *Constructive Approximation*, vol. 26, no. 2, pp. 289-315, 2007.
- [43] M. Jaderberg, K. Simonyan, A. Zisserman, K. Kavukcuoglu, "Spatial transformer networks," *NIPS*, 2015.
- [44] T. J. O'Shea, K. Karra, and T. C. Clancy, "Learning to communicate: Channel auto-encoders, domain specific regularizers, and attention," in *Proc. IEEE Int. Symp. Signal Process. and Inf. Technol. (ISSPIT)*, 2016, pp. 223-228.
- [45] T. J. O'Shea and J. Hoydis, "An introduction to deep learning for the physical layer," *IEEE Trans. Cogn. Commun. Netw.*, vol. 3, no. 4, pp. 563-575, 2017.
- [46] S. Shalev-Shwartz and S. Ben-David, *Understanding Machine Learning: From Theory to Algorithms*. Cambridge University Press, 2014.
- [47] T. J. O'Shea and N. West, "Radio machine learning dataset generation with GNU radio," in *Proc. GNU Radio Conf.*, 2016, vol. 1, no. 1.



Chieh-Fang Teng (S'17) received his B.S. degree in electrical engineering from National Taiwan University, Taipei, Taiwan, in 2017. He is currently pursuing a Ph.D. degree in the Graduate Institute of Electronics Engineering, National Taiwan University. His research interests are in the areas of Internet-of-things, VLSI architecture for DSP, and 5G wireless communication technologies with the assisted of machine learning.



Ching-Yao Chou (S'16) received the B.S. degree in electrical engineering from National Taiwan University, Taiwan, in 2014. He is currently pursuing the Ph.D. degree in the Graduate Institute of Electronics Engineering, National Taiwan University. His research focuses on low-complexity signal processing for edge analysis, trying to link compressive sensing with machine learning.



Chun-Hsiang Chen received the B.S. degree in electrical engineering from National Central University, Taoyuan, Taiwan, in 2018. He is currently pursuing the M.S. degree with the Graduate Institute of Electronics Engineering, National Taiwan University, Taipei, Taiwan. His research interests include communication systems and machine learning.



An-Yeu (Andy) Wu (M'96-SM'12-F'15) received the B.S. degree from National Taiwan University in 1987, and the M.S. and Ph.D. degrees from the University of Maryland, College Park in 1992 and 1995, respectively, all in Electrical Engineering. In August 2000, he joined the faculty of the Department of Electrical Engineering and the Graduate Institute of Electronics Engineering, National Taiwan University, where he is currently a distinguished professor. His research

interests include VLSI architectures for signal processing and communications, and adaptive/multirate signal processing. He has published more than 190 refereed journal and conference papers in above research areas, together with five book chapters and 16 granted US patents. From August 2007 to Dec. 2009, he was on leave from NTU and served as the Deputy General Director of SoC Technology Center (STC), Industrial Technology Research Institute (ITRI), Hsinchu, Taiwan. In 2010, he received "Outstanding EE Professor Award" from The Chinese Institute of Electrical Engineering (CIEE), Taiwan. From 2012 to 2014, he served as the Chair of VLSI Systems and Applications (VSA) Technical Committee (TC), one of the largest TCs in IEEE Circuits and Systems (CAS) Society. In 2015, he is elevated to IEEE Fellow for his contributions to DSP algorithms and VLSI designs for communication IC/SoC.